Korean J. Chem. Eng., 40(7), 1598-1605 (2023)
DOI: 10.1007/s11814-023-1383-5

pISSN: 0256-1115
eISSN: 1975-7220

Effect of porosity gradient in cathode gas diffusion layer on electrochemical performance of proton exchange membrane fuel cells

Guogang Yang, Hao Wang†, Fengmin Su, Shian Li, Guoling Zhang, Juncai Sun, Qiuwan Shen, Ziheng Jiang, Jiadong Liao, and Pengyu Chen

Marine Engineering College, Dalian Maritime University, Dalian 116026, China
(*Received 25 October 2022 • Revised 14 December 2022 • Accepted 20 December 2022*)

Abstract−Proton exchange nembrane fuel cells (PEMFCs) are highly promising energy devices for future transportation and distributed power stations. The electrochemical performance of PEMFCs assembled with gas diffusion layer (GDL) of different porosity gradient distributions has been analyzed using the lattice Boltzmann method. A single-phase multi-component lattice Boltzmann model employing the active approach was developed to investigate the reactive gas flow within the GDL. Two types of GDLs with the same porosity, namely multilayer porosity gradient GDLs and linear porosity gradient GDLs, were generated to investigate the effect of the porosity gradient of the GDL on the electrochemical performance of PEMFC. The results show that the two types of porosity gradient GDL improve oxygen starvation problems and enhance water management, and that the GDLs with smaller porosity gradients can increase the mean current density. This paper develops the study of pore-scale analysis of PEMFC performance and can provide guidance for the design of GDL structures.

Keywords: Gas Diffusion Layer, Porosity Gradient, Electrochemical Performance, Lattice Boltzmann Method

INTRODUCTION

Energy and environment pollution are the main challenges facing human society at present, and clean energy efficient utilization technology is an important guarantee for sustainable development. Proton exchange membrane fuel cells (PEMFCs) have been favored for their high efficiency and environmental protection, and have the advantages of high energy conversion rate, high power density, and zero-emission [1]. The gas diffusion layer (GDL) is an important component of the membrane electrode assembly in PEMFC, which acts as a carrier for water and gas transport, heat transfer, and electron conduction, and provides structural support for other components during assembly and operation [2]. Therefore, GDL directly affects the electrochemical reaction progress and the operation efficiency of the PEMFC [3].

As GDLs are porous media with complex structure and micron-scale pores, fluid flow within them cannot be regarded as continuous medium, making it difficult for macro-scale simulation methods to accurately analyze the internal flow fields. The lattice-Boltzmann method (LBM) is based on the Boltzmann equation for non-equilibrium physics and can thus be a link between the molecular scale and the macroscopic scale [4]. Some scholars have adopted LBM to study the transport properties of the GDL. The transport parameters of the GDL characterize its performance as the heat, electricity, gas, and water transport carrier, and have attracted the attention of scholars [5,6]. Fang et al. [7] evaluated the effect of different structural parameters and perforation on the permeability, effective diffusion coefficient, and effective thermal conductivity of GDL. The presence of droplets within the GDL was found to lead to an increase in tortuosity and a decrease in diffusivity [8]. The effect of porosity and fiber diameter on the anisotropic permeability of GDL was evaluated by Jiang et al. [9]. Toray TGP-H-060 and Freudenberg H2315 were reconstructed by Zhang et al. [10] who found that compression resulted in lower effective gas diffusivity and higher effective thermal and electrical conductivity. There are other researches based on LBM to study the transport properties of GDL, such as permeability [11], gas diffusivity [12], electrical conductivity [13], and tortuosity [14]. The transport of liquid water within the GDL is also of considerable interest. Yang et al. [15] found that increasing the rib width from 0.8 mm to 2 mm increased the inconsistency of liquid water distribution and the fuel cell impedance. The effects of hydrophilic fiber ratio and compression on water transport within the GDL were simulated by Ira et al. [16], who found that hydrophilic fibers lead to discontinuous water clusters and compression increases the number of discontinuous water clusters. The effects of GDL thickness and rib width on water saturation within the GDL were analyzed by Jeon et al. [17].

At present, the main methods to analyze the influence of GDL properties on fuel cell performance are mainly experimental and macroscopic simulation techniques. Lin et al. [18] measured the performance of PEMFCs assembled with compressed GDL and found that there is an optimum value of compression ratio that maximizes PEMFC power density. Wavy surface gas flow channels capable of increasing the power density of PEMFC were designed and numerically simulated by Li et al. [19]. However, GDL is a highly inhomogeneous porous medium with micron-scale pores, so pore-scale simulation methods that can capture the microstructure of GDL are more reliable, but it is currently not given enough attention. The

†To whom correspondence should be addressed.
E-mail: whdlmu@dlmu.edu.cn

distribution of water vapor, oxygen, and current density for GDLs with different fiber diameters was obtained by Bahoosh et al. [20]. Nazemian et al. found that an increase in GDL thickness led to a decrease in current density, while fiber diameter had a negligible effect on current density [21]. The reactive gas flow through the carbon cloth GDL was simulated by Molaeimanesh et al. [22], who found that the more fibers in the bundle, the lower the average current density. Due to the limitation of computational resources, the 3D numerical model can only represent the local mass transfer and electrochemical performance within the PEMFC. Therefore, the reactive gas transfer process within the cathode electrode was also investigated by the 2D model for the PEMFC with interdigitated flow field. Chen et al. [23] adopted a passive method to obtain the species distribution within the GDL and the current density distribution on the surface of the catalyst layer. The other components are treated as solutes of the main component in the passive method, whereas it will lack accuracy when the other component fractions are comparable. An active method based on multi-component multi-phase model has been developed to more accurately simulate reactive gas flow problems, based on the idea that when the number of phases is reduced to 1, the inter-particle forces that cause phase separation do not exist. The influence of inlet and outlet pressure difference, channel to rib width ratio, and flow channel width were studied by Molaeimanesh et al. [24], employing the active method and finding that increasing the pressure difference, reducing the channel to rib width ratio, and reducing the channel width can increase the current density. Bahoosh et al. [25] found that increasing the fiber diameter resulted in a more uniform distribution of oxygen, a higher current density and facilitated the removal of water vapor.

Designing GDL with porosity gradients has become one of the key research hotspots for PEMFC. Habiballahi et al. [26] found that the GDLs with smaller porosity on the side of the catalyst layer were more conducive to liquid water removal than uniformly porous GDLs, with a reduction in water saturation of over 20%. GDL with a V-shaped porosity distribution was demonstrated to remove water more quickly by Shangguan et al. [27]. Huang et al. [28] revealed that GDLs with linear porosity gradients were able to increase the PEMFC limiting current density and oxygen usage. Kanchan et al. [29] found that a reduction in GDL porosity from the gas channel to the catalyst layer resulted in the greatest current density and the smallest overpotential. The gas flow in the anode of a solid oxide fuel cell with porosity gradient was simulated by Espinoza-Andaluz et al. [30], who found that decreasing the porosity gradient in the flow direction resulted in a greater gas flow rate, facilitating the transport of reactants to the active region for reaction. In our previous study [31], we found that a suitable porosity gradient can lead to greater GDL permeability resulting in an enhanced ability for gas to pass through the GDL.

Simulation of GDL cathodic reactive gas flow based on pore-scale techniques enables a more accurate analysis of PEMFC electrochemical performance, which has not received sufficient attention. The porosity gradient distribution has been a hot topic of GDL research in recent years and has been proven to have a significant effect on the mass transfer process within GDLs. In this paper, an innovative study of the electrochemical performance of PEMFC assembled with porosity gradient GDLs has been carried out. A two-dimensional single-phase multi-component model based on the active method was developed to simulate reactive gas flow within the GDL. GDLs with linear and multilayer porosity gradient distributions were generated, with three porosity gradients of each type. The molar fraction distribution of oxygen and water vapor within each GDL was analyzed and the current density at the surface of the catalyst layer given.

MODEL DESCRIPTION

1. LB Model

To simulate single-phase multi-component gas flow, the active method developed by Molaeimanesh et al. [24] was employed for modeling reactive gas flow within the GDL. In the LBM, the fluid region is divided into regular lattices and the motion of the fluid is treated as the motion of fluid particles located at the lattice points. The LBM is based on the Boltzmann equation, which describes the evolution of particles through their collisions and streaming. The velocity distribution function is the fundamental variable of the LBM, which evolves as follows [32]:

$$f_i^k(x+c_i\Delta t,\ t+\Delta t)=f_i^k(x,\ t)+\frac{\Delta t}{\tau^k}[f_i^{k,\,eq}(x,\ t)-f_i^k(x,\ k)] \tag{1}$$

where, f_i^k is the velocity distribution function of component k at (x, t), Δt is the time step, and τ^k is the relaxation time of component k. $f_i^{k,eq}$ is the equilibrium distribution function of component k at (x, t), which can be expressed as follows:

$$f_i^{k,\,eq}=w_i\rho^k\left[1+\frac{c_i\cdot u}{c_s^2}+\frac{1}{2}\frac{(c_i\cdot u)^2}{c_s^4}-\frac{1}{2}\frac{u^2}{c_s^2}\right] \tag{2}$$

where, ρ^k is the density of component k and c_s is the lattice speed of sound. w_i and c_i are the weight factor and particle velocity vector, respectively. In the two-dimensional nine velocity (D2Q9) model, they can be given as:

$$w_i=\begin{cases}4/9 & i=1\\ 1/0 & i=2,\ 3,\ 4,\ 5\\ 1/36 & i=6,\ 7,\ 8,\ 9\end{cases} \tag{3}$$

$$[c_1\ \ c_2\ \ c_3\ \ c_4\ \ c_5\ \ c_6\ \ c_7\ \ c_8\ \ c_9]=\begin{bmatrix}0 & 1 & 0 & -1 & 0 & 1 & -1 & -1 & 1\\ 0 & 0 & 1 & 0 & -1 & 1 & 1 & -1 & -1\end{bmatrix} \tag{4}$$

The density of component k and the composite velocity can be calculated as follows:

$$\rho^k=\sum_{i=1}^{9}f_i^k(x,\ t) \tag{5}$$

$$u=\frac{\sum_{i=1}^{9}f_i^k(x,\ t)c_i}{\rho^k} \tag{6}$$

2. Computational Domain and Boundary Conditions

To investigate the reactive gas flow in the PEMFC with interdigitated flow field, a two-dimensional model containing gas channel (GC), rib, and GDL was constructed and presented in Fig. 1(a). Carbon paper GDL has a porous structure with micron-scale pores

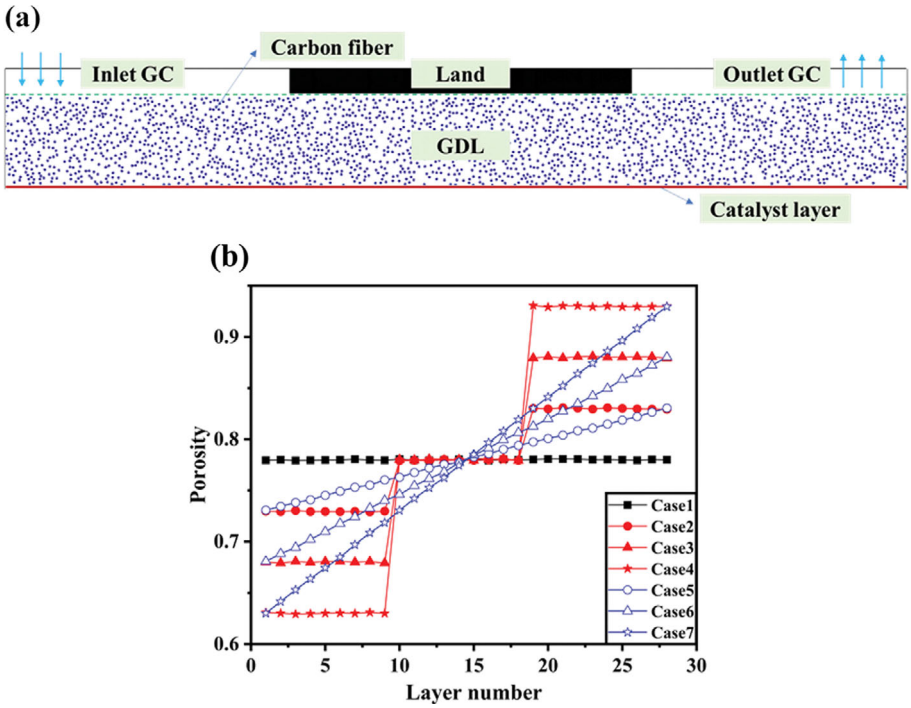

Fig. 1. (a) Computational domain scheme for the 2D LB model; (b) Local porosity of the GDLs employed in this paper.

and is composed of stacked carbon fibers. To represent the stochasticity of the carbon fiber distribution, the GDL was reconstructed based on the stochastic reconstruction method. In the two-dimensional model, the carbon fibers are simplified as cylinders with uniform diameters and are generated layer by layer [17,33]. By controlling the frequency of carbon fibers in each fiber layer, the local porosity of the GDL is specified and ultimately a porosity gradient GDL can be obtained. As the GDL performs the function of loading the catalyst, a smaller local porosity of the GDL on the catalyst layer side facilitates the catalyst loading. Two types of porosity gradient GDLs, linear type (Case 2, 3, and 4) and multilayer type (three layers, Case 4, 5, and 6), are considered and compared with the uniform GDL (Case 1). The local porosity of the GDLs employed in this paper is illustrated in Fig. 1(b). All GDLs have the same porosity of 0.78 and more computational domain parameters are listed in Table 1. Consistent with many previous studies, the total width of the computational domain was selected to be 2,000 μm, with the rib to GC width ratio of 1 : 1. Here, 1 μm equals 1 lattice unit (lu). The condensation and evaporation processes of liquid water were not considered.

Table 1. Structural and operational parameters

Parameter	Value
Width of the GC	1,000 μm
Width of the rib	1,000 μm
GDL thickness	200 μm
GDL porosity	0.78
Operating temperature	353 K
Operating pressure	1.5 atm
Oxygen molar fraction at the inlet	0.21
Nitrogen molar fraction at the inlet	0.79
Dynamic viscosity of oxygen	2.34×10^{-5} kg/(m·s)
Dynamic viscosity of nitrogen	2.01×10^{-5} kg/(m·s)
Dynamic viscosity of water vapor	1.20×10^{-5} kg/(m·s)
Diffusivity of oxygen in the mixture	1.891×10^{-5} m^2/s
Roughness coefficient	2,000
Reference current density	1.3874×10^{-2} A/m^2
Forward oxygen reduction transfer coefficients	0.5
Reverse oxygen reduction transfer coefficients	1
Overpotential	0.5 V

Dry air at a pressure of 1.5 atm with an oxygen/nitrogen molar fraction ratio of 0.21/0.79 flows through the inlet gas channel and participates in the electrochemical reaction at the surface of the catalyst layer. The pressure boundary condition proposed by Zou et al. [34] was applied to the inlet and outlet with a pressure difference of 0.01 atm. The no-slip bounce-back boundary condition was applied to solid part (rib and carbon fibers). Symmetric boundary conditions were used at the left and right boundaries.

The modified bounce-back boundary condition for reactive surface developed by Molaeimanesh et al. [24] was applied to the bottom of the computational domain, which is the catalyst layer simplified to a thin interface. When the oxygen particles hit the catalyst layer, K_{sr}^{LB} of the oxygen is consumed and converted to water, and the remaining $(1-K_{sr}^{LB})$ of the oxygen bounces back into the GDL. K_{sr}^{LB} is the electrochemical reaction rate in lattice unit and can be calculated as follows:

$$K_{sr}^{LB}=\left(\frac{6k_{sr}\Delta t}{\Delta x}\right)/\left(1+\frac{k_{sr}\Delta x}{2D}\right) \tag{7}$$

where, k_{sr} is the electrochemical reaction rate constant, Δt and

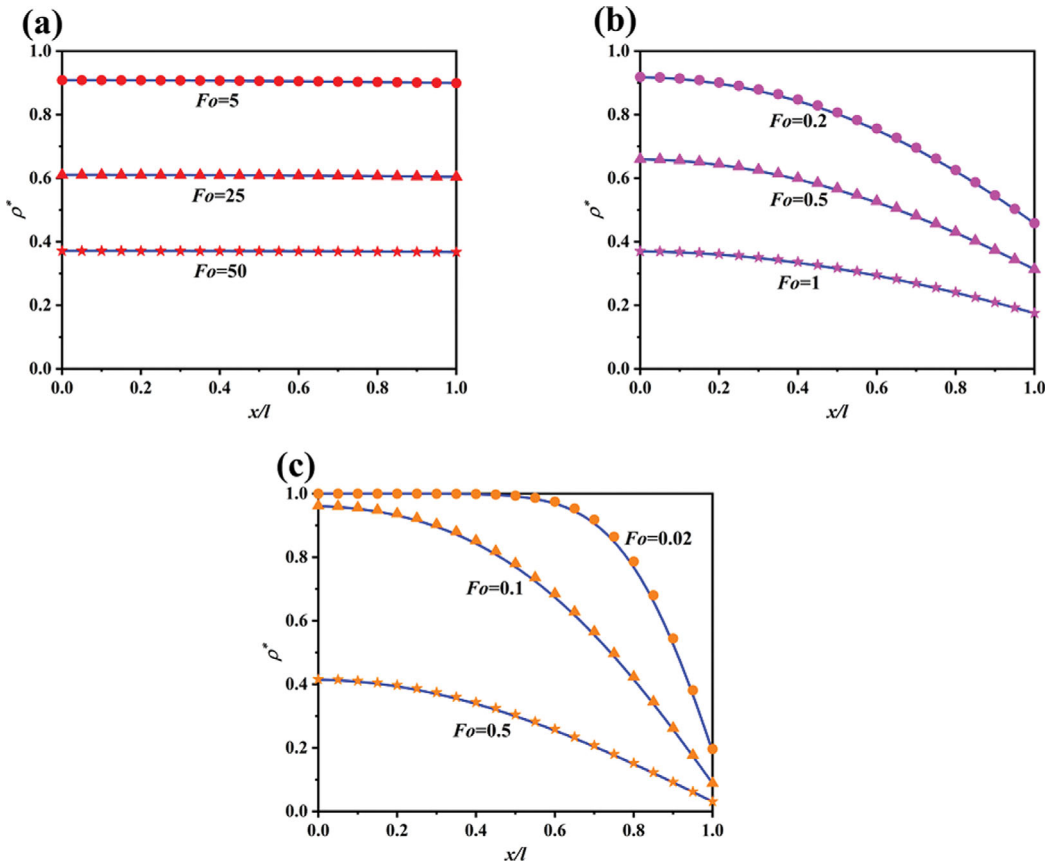

Fig. 2. Validation of the LB model for reactive surface at various Fo and Da, (a) Da=0.02, (b) Da=2, (c) Da=20; symbols: LBM results, solid lines: analytical solutions.

Δx are the time and space intervals, respectively, and D is the diffusivity of oxygen in the mixture. k_{sr} can be determined by the current density (J) and the oxygen concentration on the surface of the cathode catalyst layer (ρ_{O2}):

$$k_{sr} = \frac{J}{4F\rho_{O2}} \tag{8}$$

where, F is the Faraday constant, and J can be obtained according to the Butler-Volmer equation:

$$J = a_r J_{ref} \frac{\rho_O}{\rho_{O,ref}} \left[\exp\left(\frac{\alpha_f F \eta}{R_u T}\right) - \exp\left(-\frac{\alpha_r F \eta}{R_u T}\right) \right] \tag{9}$$

where, a_r is the roughness coefficient, J_{ref} and $\rho_{O,ref}$ are the reference current density and reference oxygen density, respectively. α_f and α_r are the forward and reverse oxygen reduction transfer coefficients, respectively. η is the activation over-potential.

To verify the established modified bounce-back boundary condition for reactive surface, the reaction-diffusion process between two infinitely long reactive surfaces is simulated and compared with the analytical solution. The analytical value of the dimensionless concentration (ρ(x, t)) distribution from the mid-line position to the reaction surface can be calculated as follows:

$$\rho(x, t) = \sum_{n=1}^{\infty} \frac{4\sin(\lambda_n)}{2\lambda_n + \sin(2\lambda_n)} e^{-\lambda_n^2 Fo} \cos\left(\lambda_n \frac{x}{l}\right) \tag{10}$$

where, $Fo = Dt/l^2$ is the Fourier number, which can be regarded as dimensionless time. λ_n is the root of the equation $\lambda_n \tan(\lambda_n) = Da$. $Da = lk_{sr}/D$ denotes the Damköhler number. The comparison between the LBM results and the analytical solution obtained by selecting several sets of Da and Fo is shown in Fig. 2. It is obvious that the LBM results are in good agreement with the analytical solution, which proves the feasibility of the surface reaction model established in this paper.

The distribution of reactive gases within the GDL is considered to have reached a steady state if the relative error of the current density on the surface of the catalytic layer is less than 10^{-6} for 200 consecutive steps.

RESULTS AND DISCUSSION

To evaluate the electrochemical performance of porosity gradient GDLs, two types of porosity gradient distributions, linear and multilayer type, were considered, with three porosity gradients considered in each type. The molar fraction distribution of oxygen, water vapor within each GDL was analyzed and the current density given. The current density distribution on the catalyst layer surface obtained after simulating reactive gas flow within the porosity uniform GDL was compared with the results of previous studies and is presented in Fig. 3. As can be seen, the current density distribution obtained is very close to that reported in the literature,

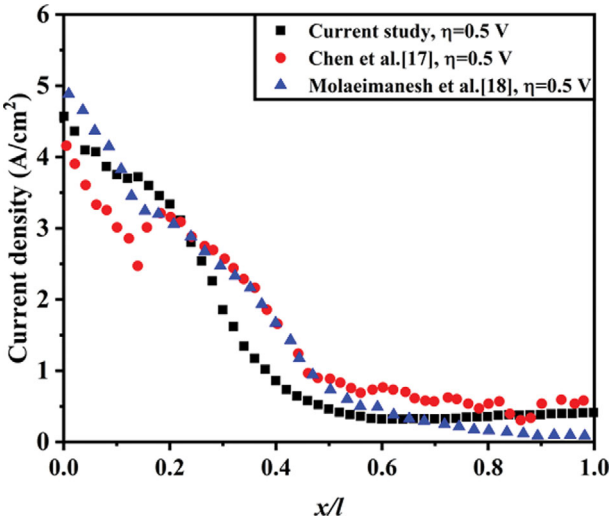

Fig. 3. Distribution of current density on the catalyst layer surface of the GDL with uniform porosity.

and the differences are due to the difference in the structure of the GDL. From the gas inlet to the outlet, the local current density gradually decreases as oxygen is consumed. At x/*l*>0.25, the rate of decrease in current density accelerates, which is due to the reduced oxygen supplementation capacity caused by the obstructive effect of the rib on the inlet gas. At x/*l*>0.5, the current density distribution stabilizes, indicating that the oxygen has been almost depleted. In subsequent work, GDL with uniform porosity will be used as base case for comparison with other porosity gradient GDLs.

The molar fraction distribution of oxygen within multilayer porosity gradient GDLs is shown in Fig. 4. Due to oxygen being consumed at the catalyst layer, the molar fraction of oxygen decreases significantly from the gas inlet to the outlet. As shown in the area circled by the red line, oxygen-poor regions are formed in the lower right corner of the computational domains, where the molar fraction of oxygen is less than 0.01, as oxygen is difficult to be replenished as adequately as in the area below the inlet GC. As shown in Fig. 4(b), 4(c), and 4(d), there is a significant reduction in the area of oxygen-poor regions within the multilayer porosity gradient GDLs compared to the area within the porosity uniform GDL. Compared to Case1, Case2, Case3, and Case4 having 51.42%, 68.97%, and 81.49% less oxygen-poor regions respectively, due to the larger local porosity of the upper part of the multilayer porosity gradient GDLs which is more conducive to oxygen transport to the exit side, allowing oxygen to diffuse to the catalyst layer surface. The reduction of the oxygen-poor region means that multilayer type porosity gradient GDLs can further alleviate the problem of oxygen starvation within the GDL.

The molar fraction distribution of water vapor within multilayer porosity gradient GDLs is shown in Fig. 5. Water vapor is generated at the surface of the catalyst layer and driven by the flowing gas within the GDL, resulting in a higher molar fraction of water vapor near the outlet. Water management issues are a key factor in the operation of fuel cell systems. The accumulation of excess water vapor can lead to the generation of liquid water blocking the gas flow paths and untimely drainage of water vapor or liquid water is a major cause of flooding. Water vapor accumulates in the lower right corner of the computational domain to form a water-rich region, and the area of the water-rich region within the multilayer porosity gradient GDL is significantly smaller than that within the

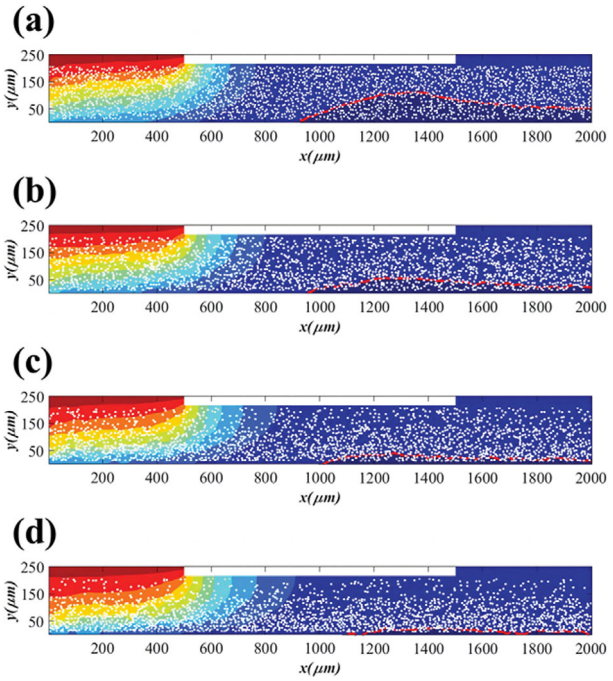

Fig. 4. The molar fraction distribution of oxygen within multilayer porosity gradient GDLs and porosity uniform GDL, (a) Case1, (b) Case2, (c) Case3, and (d) Case4.

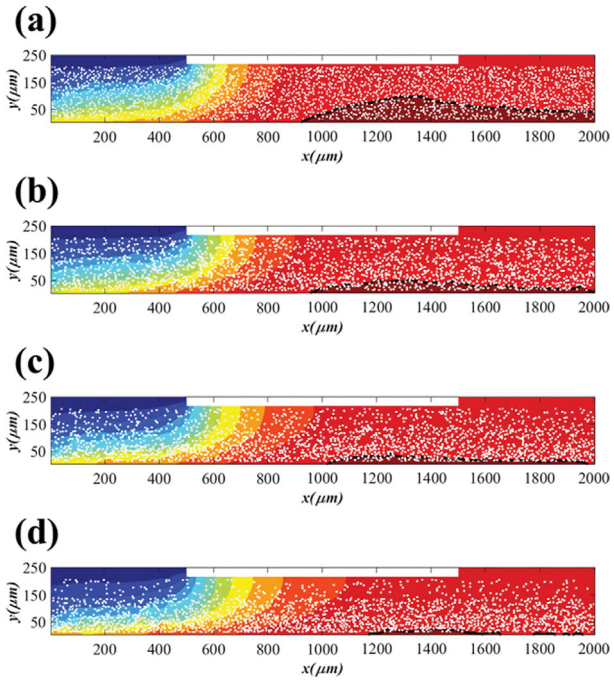

Fig. 5. The molar fraction distribution of water vapor within multilayer porosity gradient GDLs and porosity uniform GDL, (a) Case1, (b) Case2, (c) Case3, and (d) Case4.

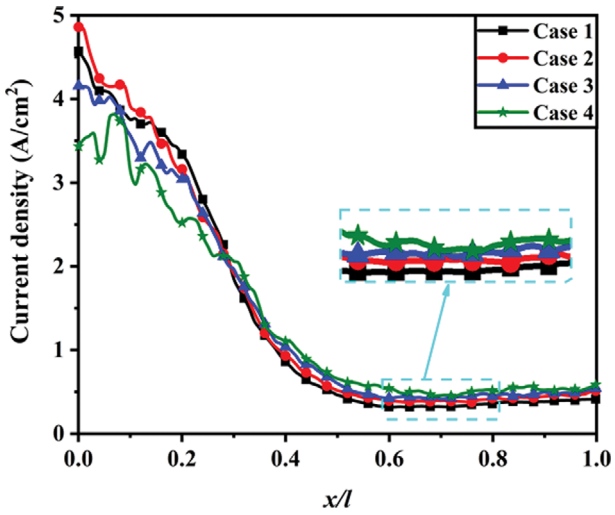

Fig. 6. Current density distribution on the catalyst layer surface for multilayer porosity gradient GDLs and porosity uniform GDL.

Table 2. The mean current density for multilayer porosity gradient GDLs and porosity uniform GDL

	Case1	Case2	Case3	Case4
Mean current density (A/cm^2)	1.4135	1.4630	1.4330	1.3822

porosity uniform GDL. More specifically, for Case2, Case3, and Case4, the area of water-rich region is reduced by 52.55%, 71.31%, and 86.99% respectively, indicating that multilayer porosity gradient GDLs can be adopted to improve water management.

Current density distribution on the catalyst layer surface for multilayer porosity gradient GDLs and porosity uniform GDL is shown in Fig. 6. The obvious difference occurs at the stage where $x/l<0.25$, which is below the inlet GC. The smaller local porosity of the GDL on the catalyst layer side increases the difficulty of downward gas transport and permeation, so that the local current density of Case4 is lowest below the inlet GC. In the $x/l>0.25$ region the local current density is much closer in the four cases. Whereas in the current density stability region of $x/l>0.5$, the reduction in the area of the oxygen-poor region within the multilayer type porosity gradient GDL implies a higher oxygen concentration on the catalyst layer surface, which in turn results in a greater local current density. The mean current density for multilayer porosity gradient GDLs and porosity uniform GDL is listed in Table 2. The mean current density of Case2 and Case3 is 3.50% and 1.38% higher than that of Case1, respectively, indicating that multilayer porosity gradient GDLs can weaken oxygen starvation and improve PEMFC performance through enhanced mass transport at smaller porosity gradients. In contrast, the average current density of Case4 is reduced by 2.22% compared to that of Case1. Although the oxygen-poor region within the GDL is relatively reduced, it is more difficult for oxygen to reach the surface of the catalyst layer below the inlet GC due to the obstructive effect of the fibers near the catalyst layer, resulting in lower overall performance.

The molar fraction distribution of oxygen within linear porosity gradient GDLs and porosity uniform GDL is presented in Fig.

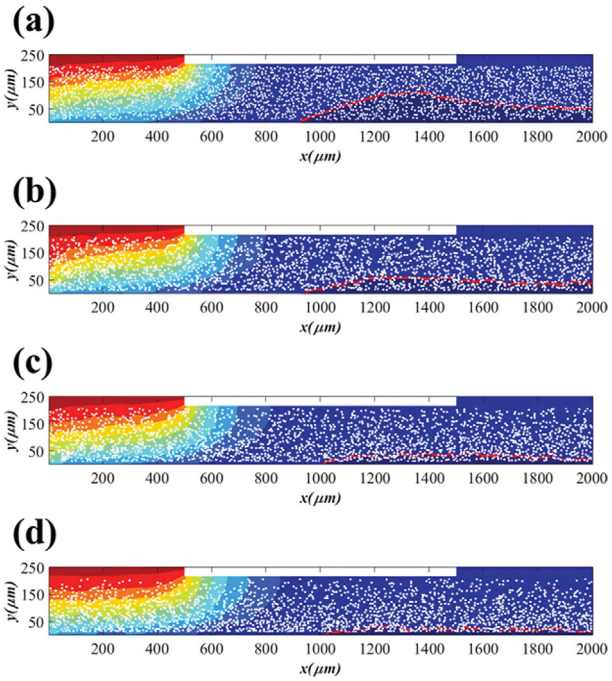

Fig. 7. The molar fraction distribution of oxygen within linear porosity gradient GDLs and porosity uniform GDL, (a) Case1, (b) Case5, (c) Case6, and (d) Case7.

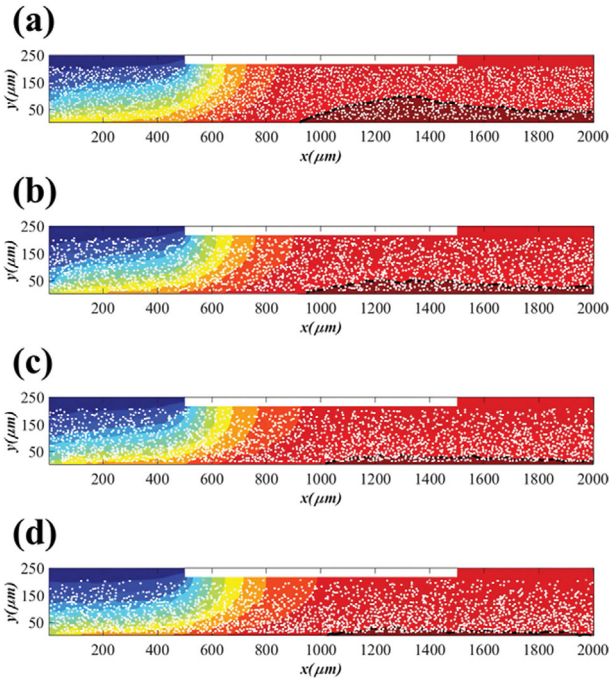

Fig. 8. The molar fraction distribution of water vapor within linear porosity gradient GDLs and porosity uniform GDL, (a) Case1, (b) Case5, (c) Case6, and (d) Case7.

7, which is similar to that in multilayered porosity gradient GDLs. The linear porosity gradient distribution also contributes to weakening the oxygen starvation problem, with Case5, Case6 and Case7 having 42.47%, 64.10% and 73.88% less oxygen-poor region area,

respectively, compared to Case1. The local porosity of the linear porosity gradient GDL near the GC side is less than that of the multilayer porosity gradient GDL, so the oxygen transport capacity along the *x*-direction is slightly lower, and the weakening capacity of the area in the oxygen-poor region is less than that of the multilayer porosity gradient GDL. Given in Fig. 8 is the water vapor molar fraction distribution within a linear porosity gradient GDLs and porosity uniform GDL. Water vapor similarly converges towards the outlet GC and forms a water-rich region in the lower right-hand corner of the computational domain. For Case5, Case6 and Case7, reductions of 43.87%, 65.24% and 74.73% in the area of the water-rich region can be observed, respectively, indicating that the linear porosity gradient GDL has the ability to improve water management, but is inferior to the multilayer porosity gradient GDL.

Depicted in Fig. 9 is the current density distribution on the catalyst layer surface for linear porosity gradient GDLs and porosity uniform GDL. The greater variability in current density for the four cases still occurs below the inlet GC. Case7 has the lowest local current density in the $x/l<0.25$ region, demonstrating that a large porosity gradient significantly prevents oxygen from penetrating downwards. The illustration in Fig. 9 shows that a linear porosity gradient GDL improves the electrochemical performance in the $x/l>0.5$ region. Since the local porosity of the GDL on the GC side is greater than on the catalyst side, oxygen will flow horizontally when downward penetration is impeded and then continue to penetrate into the catalyst layer, allowing more oxygen to be available in the $x/l>0.5$ region. The average current density of the linear porosity gradient GDLs is given in Table 3. the average current density of Case5, Case6 and Case7 is 3.29%, 2.97% and 1.80% higher than that of Case1, respectively. Linear porosity gradient GDLs can enhance PEMFC performance; however, considering the difficulty of the GDL preparation process, multilayer type porosity gradient GDLs can be produced by laminating three thin GDLs with different porosities, whereas linear porosity gradient GDL are still challenging to manufacture with the current technology. Therefore, multilayer porosity gradient GDLs should be a more achievable option to improve oxygen starvation and water management within the GDL and enhance PEMFC performance.

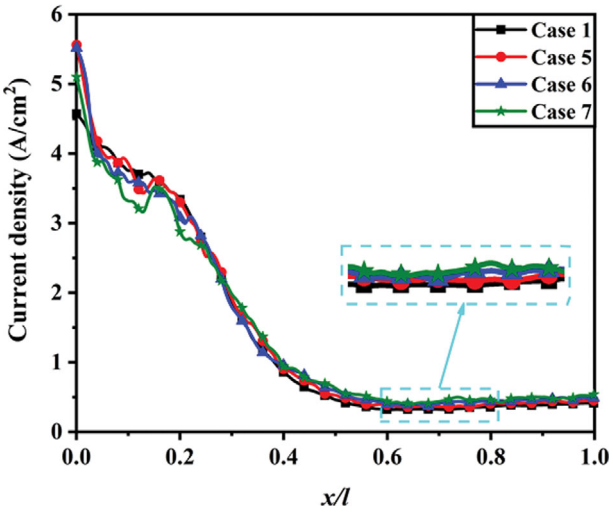

Fig. 9. Current density distribution on the catalyst layer surface for linear porosity gradient GDLs and porosity uniform GDL.

Table 3. The mean current density for linear porosity gradient GDLs and porosity uniform GDL

	Case1	Case5	Case6	Case7
Mean current density (A/cm^2)	1.4135	1.4600	1.4555	1.4389

CONCLUSIONS

A single-phase multi-component LB model was developed to investigate the effect of multilayer and linear porosity gradient GDL on the electrochemical performance of PEMFC. The main factors--oxygen, water vapor molar fraction distribution and current density distribution within the porosity gradient GDL--were analyzed. More specific conclusions are given as follows:

(1) As oxygen was consumed in the catalyst layer, an oxygen-poor region was formed at the lower right corner of the computational domain. Both the multilayer porosity gradient GDL and the linear porosity gradient GDL reduced the area of the oxygen-poor region, indicating that the porosity gradient GDL can be used to improve the oxygen starvation.

(2) Water vapor was generated in the catalyst layer and was driven by the flowing gas to accumulate near the outlet GC and form a water-rich region. The water-rich region areas within the porosity gradient GDL were significantly reduced, indicating that water vapor within the porosity gradient GDL can be removed more quickly and that the porosity gradient GDL has the ability to improve water management.

(3) The mean current density for Case2 of the multilayer porosity gradient GDL was 3.5% higher than that of the porosity uniform GDL, while the mean current density of Case4 was 2.22% lower, indicating that the smaller porosity gradient of GDL contributes to improved PEMFC performance.

(4) The mean current densities of the linear porosity gradient GDLs were all higher than those of the porosity uniform GDL.

ACKNOWLEDGEMENTS

This work is supported by the National Natural Science Foundation of China (No. 51779025 and No. 52001045), Science and Technology Innovation Foundation of Dalian, China (No. 2021 JJ11CG004). Particularly, thanks for Huixin Guo's help.

DECLARATION OF COMPETING INTEREST

The authors declare that they have no known competing financial interests or personal relationships that could have appeared to influence the work reported in this paper.

REFERENCES

1. S. Wu, W. Yang, J. Zhan, H. Yan, X. Kon and X. Zuo, *Korean J. Chem. Eng.*, **39**, 2055 (2022).
2. D. Joo, K. Han, J. H. Jang and S. Park, *Korean J. Chem. Eng.*, **36**,

299 (2019).
3. G. R. Molaeimanesh, M. H. Shojaeefard and M. R. Moqaddari, *Korean J. Chem. Eng.*, **36**, 136 (2019).
4. A. K. Hussein, H. K. Hamzah, F. H. Ali and M. Afrand, *Korean J. Chem. Eng.*, **39**, 887 (2022).
5. D. Zhang, Q. Cai and S. Gu, *Electrochim. Acta*, **262**, 282 (2018).
6. D. Froning, J. Brinkmann, U. Reimer, V. Schmidt, W. Lehnert and D. Stolten, *Electrochim. Acta*, **110**, 325 (2013).
7. W.-Z. Fang, Y.-Q. Tang, L. Chen, Q.-J. Kang and W.-Q. Tao, *Int. J. Heat Mass Transf.*, **126**, 243 (2018).
8. M. Espinoza-Andaluz, R. Reyna, A. Moyón, T. Li and M. Andersson, *Int. J. Hydrogen Energy*, **45**, 29824 (2020).
9. Z. Jiang, G. Yang, S. Li, Q. Shen, J. Liao, H. Wang, M. Espinoza-Andaluz, R. Ying and X. Pan, *Comput. Mater. Sci.*, **190**, 110286 (2021).
10. H. Zhang, L. Zhu, H. B. Harandi, K. Duan, R. Zeis, P.-C. Sui and P.-Y. A. Chuang, *Energy Conv. Manag.*, **241**, 114293 (2021).
11. Y. Gao, T. Jin, X. Wu and T. Zhang, *Energies*, **12**, 2808 (2019).
12. P. A. García-Salaberri, I. V. Zenyuk, A. D. Shum, G. Hwang, M. Vera, A. Z. Weber and J. T. Gostick, *Int. J. Heat Mass Transf.*, **127**, 687 (2018).
13. L. Zhu, H. Zhang, L. Xiao, A. Bazylak, X. Gao and P.-C. Sui, *J. Power Sources*, **496**, 229822 (2021).
14. A. Nabovati, J. Hinebaugh, A. Bazylak and C. H. Amon, *J. Power Sources*, **248**, 83 (2014).
15. M. Yang, Y. Jiang, J. Liu, S. Xu and A. Du, *Int. J. Hydrogen Energy*, **47**, 10366 (2022).
16. Y. Ira, Y. Bakhshan and J. Khorshidimalahmadi, *Int. J. Hydrogen Energy*, **46**, 17397 (2021).
17. D. H. Jeon, *J. Power Sources*, **475**, 228578 (2020).
18. J.-H. Lin, W.-H. Chen, Y.-J. Su and T.-H. Ko, *Fuel*, **87**, 2420 (2008).
19. S. Li, J. Yuan, M. Andersson, G. Xie and B. Sundén, *J. Electrochem. Energy Convers. Storage*, **14**, 031007 (2017).
20. R. Bahoosh, M. Jafari and S. S. Bahrainian, *Korean J. Chem. Eng.*, **38**, 1703 (2021).
21. M. Nazemian and G. R. Molaeimanesh, *Acta Mech. Sin.*, **36**, 367 (2020).
22. G. R. Molaeimanesh and M. Dahmardeh, *Fuel Cells*, **21**, 208 (2021).
23. L. Chen, H.-B. Luan, Y.-L. He and W.-Q. Tao, *Int. J. Therm. Sci.*, **51**, 132 (2012).
24. G. R. Molaeimanesh and M. H. Akbari, *Korean J. Chem. Eng.*, **32**, 397 (2015).
25. R. Bahoosh, M. Jafari and S. S. Bahrainian, *J. Heat Mass Transf. Res.*, **6**, 105 (2019).
26. M. Habiballahi, H. Hassanzadeh, M. Rahnama, S. A. Mirbozorgi and E. J. Javaran, *Proc. Inst. Mech. Eng. Part A-J. Power Energy*, **235**, 546 (2021).
27. X. Shangguan, Y. Li, Y. Qin, S. Cao, J. Zhang and Y. Yin, *Electrochim. Acta*, **371**, 137814 (2021).
28. Y.-X. Huang, C.-H. Cheng, X.-D. Wang and J.-Y. Jang, *Energy*, **35**, 4786 (2010).
29. B. K. Kanchan, P. Randive and S. Pati, *Int. J. Hydrogen Energy*, **45**, 21836 (2020).
30. M. Espinoza, B. Sundén and M. Andersson, *ECS Trans*, **78**, 2785 (2017).
31. H. Wang, G. Yang, S. Li, Q. Shen, J. Liao, Z. Jiang, M. Espinoza-Andaluz, F. Su and X. Pan, *Int. J. Hydrogen Energy*, **46**, 22107 (2021).
32. H. Wang, G. Yang, S. Li, Q. Shen, J. Liao, Z. Jiang, G. Zhang, H. Zhang and F. Su, *Energy Fuels*, **35**, 15058 (2021).
33. Y. Ira, Y. Bakhshan and J. Khorshidimalahmadi, *Proc. Inst. Mech. Eng. Part A-J. Power Energy*, **236**, 61 (2022).
34. Q. Zou and X. He, *Phys. Fluids*, **9**, 1591 (1997).